Dinuclear LnIII Complexes with 9-Anthracenecarboxylate Showing Field-Induced SMM and Visible/NIR Luminescence

Berta Casanovas,[a] Saskia Speed,[a,b] Olivier Maury,[b] Mohamed Salah El Fallah,[a] Mercè Font-Bardía,[c] and Ramon Vicente*[a]

[a] Departament de Química Inorgànica i Orgànica, Secció de Química Inorgànica, Universitat de Barcelona, Martí i Franquès 1-11, 08028 Barcelona, Spain
http://www.ub.edu/inorgani/recerca/MagMol/magmol.htm
[b] Univ. de Lyon, UMR 5182–CNRS–Ecole Normale Supérieure de Lyon,
Universtité de Lyon 1,
46 allée d'Italie, 69007 Lyon, France
[c] Departament de Mineralogia, Cristallografia i Dipòsits Minerals and
Unitat de Difracció de R-X. Centre Científic i Tecnològic de la Universitat
de Barcelona (CCiTUB), Universitat de Barcelona,
Solé i Sabarís 1-3. 08028 Barcelona, Spain
Supporting information and ORCID(s) from

Ramon Vicente :rvicente@ub.edu

ABSTRACT:

The reaction of several Ln(NO3)3·6H2O salts with 9-anthracenecarboxylic acid (9-HAC) and 2,2′-bipyridine (bpy) in a mixture of CH3OH/H2O has allowed the isolation of the dinuclear compounds 1–6 with formula [Ln2(μ2–9-AC)4(9-AC)2(bpy)2] [LnIII = Nd (1), Eu (2), Gd (3), Tb (4), Er (5), and Yb (6)]. The molar magnetic susceptibility measurements of 1–6 in the 2–300 K temperature range indicate weak antiferromagnetic ex-. change for the isotropic GdIII compound 3. Compounds 1, 5, and 6 exhibit field-induced single-molecule magnet (SMM) behavior. The luminescence properties of compounds 1–6 in the solid state have been studied at different temperatures and show sensitization of the 4f–4f emission bands in the NIR range for compounds 1, 5, and 6.

INTRODUCTION

Lanthanide-based coordination compounds are currently of great interest for the synthesis of novel molecular materials with interesting physicochemical properties, in particular, magnetic and luminescent properties.[1–3] From a magnetic point of view, the 4f electrons in LnIII ions are efficiently shielded by the fully occupied 5s and 5p orbitals. Thus, the electronic structures of these ions are largely unaffected by the ligand field and present, in general, unquenched orbital angular momentum and significant spin–orbit coupling that yield large magnetic anisotropy and large magnetic moments in the ground state.[4] As a consequence of the above, LnIII ions are ideal candidates to form complexes that could behave as single-molecule magnets (SMMs).[5] SMMs show slow relaxation of magnetization and have potential applications in quantum computing,[6] high density data storage,[7] and spintronics.[8] The energy barrier (Ea) that prevents spin reversal in SMM compounds is proportional to the local anisotropy of the LnIII ions.[9] Due to strong spin–orbit coupling, the magnetic anisotropy of lanthanide ions is extremely sensitive to the shape and nature of the electrostatic ligand field around the ion.[4]

On the basis of previously published work, TbIII, DyIII, and ErIII ions seem to be the best candidates to obtain complexes with SMM properties, because they can present large angular and magnetic moments in the ground state.[10–15] The recently published review by Pointillart et al. highlights the viability of CeIII, NdIII, HoIII, TmIII, and YbIII ions to also form lanthanide-based SMMs.[16–18] Moreover, recent studies have revealed that strong magnetic exchange in dinuclear 4f compounds could enhance the SMM properties suppressing the quantum tunneling of magnetization (QTM) relaxation pathway.[19–21]

Furthermore, the well-shielded electronic configuration of lanthanide ions confers on them characteristic luminescence emission properties. However, due to the low extinction coefficients of the Laporte-forbidden f–f transitions, LnIII ions must be indirectly excited by energy-transfer processes from organic ligands or “antennas” that possess a large extinction coefficient (ε).[22,23] The excitation energy is then emitted as characteristic narrow f–f emission bands in the visible and/or near infra-red (NIR) spectral regions. Complexes in which ligands sensitize NIR LnIII (e.g., ErIII, NdIII, and YbIII) f–f emissions are of high interest for optical communications[24] as well as biological and sensor applications.[22]

In order to isolate discrete 4f-metal-ion complexes, such as dinuclear entities, a successful synthetic approach to follow is the simultaneous employment of bidentate bridging anionic groups and chelating neutral capping organic ligands. For the anionic species, carboxylate ligands have been widely used due to the ability of carboxylate groups to interact with LnIII ions.[17,18,25,26] On the other hand, chelating ligands could block two or three coordination sites per LnIII ion, thereby preventing potential polymerization.[27] For this purpose, N-donor species such as 2,2′-bipyridine, 1,10-phenanthroline, or 2,2′:6′,2″-terpyridine are ideal candidates.[28–32]

In addition to the synthetic advantages, the anionic derivative of 9-anthracenecarboxylic acid (9-HAC) can act as an an tenna, efficiently sensitizing the NIR emission of some LnIII ions.[33–35] Considering the aspects stated above, we aimed to synthesize multifunctional dinuclear lanthanide complexes with photoluminescence and SMM properties by using 9-HAC and 2,2′-bipyridine (bpy) ligands. The synthesis of molecular complexes displaying these two properties is currently an interesting field of research due to the potential applications of these systems in, for example, information storage, sensing, and bioimaging.[36,37] We present here six new homodinuclear compounds with the same general formula [Ln2(μ2-9-AC)4(9-AC)2(bpy)2] [LnIII = Nd (1), Eu (2), Gd (3), Tb (4), Er (5), and Yb (6)]. The crystal structure of the analogous lanthanum complex [La2-(μ2-9-AC)4(9-AC)2(bpy)2] has previously been published.[38] Moreover, recently, Zhang and Liu and co-workers reported the analogous dysprosium SMM compound [Dy2(μ2-9-AC)4(9-AC)2-(bpy)2] in order to study the magnetic dependence on the variation of the chelating N-donor ligand.[29] We wished to expand on these previous works by using other lanthanide ions in the search for multifunctional complexes displaying magnetic and luminescent properties. Thus, herein we present the syntheses, X-ray crystal structures, and magnetic and luminescent properties of complexes 1–6.

RESULTS AND DISCUSSION

Syntheses

The dinuclear lanthanide complexes 1–6 were obtained based on the previously proposed synthetic procedure for the [La2(μ2-9-AC)4(9-AC)2(bpy)2] compound.[38] A mixture of 9-anthracenecarboxylic acid (0.05 mmol) and 2,2′-bipyridine (0.05 mmol) in the presence of pyridine (0.05 mL) in methanol (10 mL) was slowly diffused into a test-tube containing a solution of the corresponding Ln(NO3)3·nH2O salt (0.1 mmol) in water (15 mL).
Yellow single crystals of the complexes suitable for X-ray analysis appeared after a few days.
The previously reported [Dy2(μ2-9-AC)4(9-AC)2(bpy)2] was synthesized under solvothermal conditions, but it could also be obtained by using this approach. Therefore, the viability of simple room-temperature synthetic procedures to obtain discrete LnIII coordination compounds is worthy of note.

X-ray Crystal Structures of 1–6

From the X-ray diffraction data it is revealed that 1–6 crystallize in the triclinic space group F(000) (Table 1). Despite the molecular structures of 1–6 being very similar, it should be noted that these complexes are not isomorphous systems, in contrast to other families of lanthanide complexes. In view of the similarity of the molecular structures of 1–6, only the structure of 1 will be described as a representative example.

[Nd2(μ2-9-AC)4(9-AC)2(bpy)2] (1)

The structure of the dinuclear compound 1 is shown in Figure 1a and selected bond lengths are listed in Table 2. The structure consists of a centrosymmetric [Nd2(μ2-9-AC)4(9-AC)2-(bpy)2] dinuclear molecule in which each NdIII ion is nine-coor dinate. The coordination sphere NdN2O7 is formed by two N atoms from one chelating bpy ligand with the Nd1–N1 and Nd1–N2 distances being 2.6744(18) and 2.6580(18) Å, respectively, two O atoms from a chelating 9-AC ligand (Scheme 1c) with Nd1–O5 and Nd1–O6 distances of 2.4544(16) and 2.4897(14) Å, respectively, and five O atoms from four 9-AC bridging ligands. These ligands present two different kinds of coordination: The symmetrical syn,syn bridge (μ2-η1:η1 or 2.11 by using Harris notation) and the chelating bridge (μ2-η2:η1 or 2.21), represented in Scheme 1a and 1b, respectively. For the syn,syn 9-AC bridging ligands, the Nd1–O1′ and Nd1–O2 bond lengths are 2.3856(14) and 2.4388(15) Å, respectively. On the other hand, the chelating-

bridge mode of 9-AC ligands presents two different Nd1–O3 distances of 2.3910(15) and 2.6074(15) Å and a Nd1–O4 bond length of 2.6436(16) Å with the Nd1–O3–Nd1′ angle of 106.7(5)°. The Nd1···Nd1′ intramolecular distance is 3.9959(3) Å. The calculated degree of distortion of the NdN2O7 coordination polyhedron of 1 (Figure 1b) with respect to the ideal nine-vertex polyhedra, as determined by continuous shape measure analysis using the SHAPE software,[39,40] shows intermediate distortion between various coordination polyhedra. The lowest continuous shape measures (CShMs) for compound 1 correspond to Muffin (MFF-9), spherical capped square antiprism (CSAPR-9), and spherical tricapped trigonal prism (TCTPR-9) with values of 1.867, 1.889, and 2.694, respectively. The values of the CShMs for complexes 1–6 are listed in Table S1 in the Supporting Information.

For compounds 1, 2, and 4–6, the dinuclear units are arranged through intermolecular π-stacking interactions between the anthracene rings of the chelating-bridging carboxylate ligands of two adjacent molecules along the [101] direction. Moreover, π-stacking interactions between adjacent chelating 9-AC ligands along the [111] direction for 1 and the [001] direction for 2 and 4–6 lead to a supramolecular 2D arrangement in the (111) plane for 1 and the (011) plane for 2 and 4–6 (Figure 2).

In the case of compound 3, a 2D supramolecular structure in the (011) plane is also observed. It is formed through π-stacking interactions between adjacent chelating 9-AC ligands along the [001] direction and by another two 9-AC ligands with a syn,syn coordination mode along the [010] direction (see Figure S1 in the Supporting Information). The centroid–centroid distances of all the complexes are collected in Table S2.

dc Magnetic Susceptibility Studies

Static magnetic measurements were collected on loose polycrystalline powder samples of complexes 1–6 in the temperature range of 2–300 K under applied fields of 0.3 T (for 1, 3, 4, and 6) and 0.5 T (2 and 5). The data for 1–6 are plotted as MT versus T in Figure 3a. The room-temperature MT values for 1–6 are 3.31, 2.86, 16.03, 25.57, 18.25, and 5.07 cm3 K mol–1, respectively. Based on the expected values for two isolated LnIII ions, the following MT values were calculated:[10] NdIII ground state 4I9/2 and gJ = 8/11, MTcalcd. = 3.28 cm3 K mol–1; EuIII ground state 7F0, MTcalcd. = 0 cm3 K mol–1; GdIII ground state 8S7/2, gJ = 2, MTcalcd. = 15.75 cm3 K mol–1; TbIII ground state 7F6, gJ = 3/2, MTcalcd. = 23.64 cm3 K mol–1; ErIII ground state 4I15/2, gJ = 6/5, MTcalcd. = 22.96 cm3 K mol–1; YbIII ground state 2F7/2, gJ = 8.7, MTcalcd. = 5.14 cm3 K mol–1. The experimental MT values are in good agreement with the calculated ones, except for compounds 2 and 5. Although the magnetic ground state of EuIII is 7F0, a non-zero experimental value of MT ≈ 2.86 cm3 K mol–1 is observed because of the second-order effect due to Zeeman-induced mixing of the close-lying excited state in the ground state.[41] The low MT value observed for compound 5 may indicate the presence of magnetic anisotropy in this compound. Upon cooling, different behavior was observed for the

different compounds. For 1, 2, and 6, the MT values slightly decrease, mainly due to the thermal depopulation of the Stark sublevels combined with a significant magnetic anisotropy.[42] At 2.0 K, the MT values are 1.29, 0.03, and 3.00 cm3 K mol–1 for 1, 2, and 6, respectively, which indicates an mJ = 0 ground sublevel for EuIII (7F0). For 3, the MT product remains almost constant until T = 9 K, and then drops to 13.07 cm3 K mol–1 at 2 K. Because GdIII has no orbital angular momentum contribution, it is not affected by spin–orbit coupling.[43] Therefore, the exchange interaction between the two GdIII in the molecule can be described by the Heisenberg–Dirac–Van Vleck (HDVV) spin Hamiltonian:[44] It is not possible to apply Equation (1) to the other LnIII because they need much more complex models based on explicit ligand-field and spin–orbit parameters.[45] Fitting of the experimental MT data for 3 reveals a weak antiferromagnetic exchange parameter J = –0.05 cm–1 with g = 2.02, which are in good agreement with previously reported values for other similar dinuclear GdIII compounds.[27,46]

$$H = -JS_1S_2 \quad (1)$$

Compound 4 shows almost constant values of MT until 13 K and then the curve slightly increases up to 27.08 cm3 K mol–1 at 6 K. At lower temperatures, the curve drops arriving at 24.26 cm3 K mol–1 at 2 K. This behavior suggests a possible competition between ferromagnetic and antiferromagnetic interactions between the TbIII ions.

In the case of compound 5, the MT values gradually decrease upon cooling. At 2 K the curve drops to a MT value of 7.30 cm3 K mol–1. As for compounds 1, 2, and 6, this behaviour is mainly a consequence of the thermal depopulation of lowlying crystal-field states and the magnetic anisotropy of ErIII ions and/or due to weak antiferromagnetic interactions between the ions.

The magnetization with increasing field for 1 and 3–6 at 2 K are depicted in Figure 3b. The GdIII complex 3 shows a saturation value of 14.11 NμB under an applied field of 5 T, which corresponds to the expected value for two weakly coupled GdIII ions (14 NμB).[47] The magnetization in compounds 1 and 4–6 increases with field up to 2.57, 10.97, 7.41, and 3.49 NμB, respectively, at the highest applied magnetic field, but without saturation, which indicates again the presence of magnetic anisotropy and/or partially populated excited states.

ac Magnetic Susceptibility Studies

Dynamic magnetic studies on compounds 1 and 4–6 were performed in order to study whether they present SMM behavior. The measurements reveal that at zero static external magnetic field none of the complexes show out-of-phase (M″) signals of ac susceptibility at frequencies up to 1488 Hz. This fact may indicate a low magnetic anisotropy or that at zero dc field the QTM process dominates the

magnetization relaxation time (τ), but this process can be suppressed or partially suppressed at low temperatures when a static magnetic field is applied.[47,48]

For 1, 5, and 6, the frequency dependence of M″ reveals temperature-dependent peaks when a dc field of 0.2 (1), 0.1 (5), or 0.05 T (6) is applied under a 4 × 10–4 T ac field oscillating at frequencies between 1–1488 Hz for 1 and 6 and between 10–1488 Hz for 5 in the temperature range of 1.8–5.5 K for 1, 1.8–3.5 K for 5, and 1.8–4.5 K for 6 (Figure 4a,d,g, respectively). In the case of compound 4, under an applied dc field of 0.15 T, a slight frequency and thermal dependency of M′ and/or M″ is observed but without net maxima (see Figure S2 in the Supporting Information).

The ac susceptibility frequency dependencies of both M′ and M″ were analyzed for 1, 5, and 6 by using the generalized Debye model.[49] The corresponding Cole–Cole plots (Figure 4b,e,h) estimate α values close to zero, which reveals that a single relaxation time is mainly involved in the relaxation process in these compounds.[50] The relaxation parameters obtained from the best fits are summarized in Tables S3–S5 in the Supporting Information.

The temperature dependence of the relaxation times (τ; Figure 4c,f,i) shows that at temperatures above 3.0 K for 1, 2.0 K for 5, and 2.7 K for 6, the variation in τ follows the Arrhenius law [$\tau = \tau_0 \exp(-U_{eff}/kBT)$], leading to effective energy barriers of 8.0, 5.6, and 16.4 cm–1 for 1, 5, and 6, respectively, and preexponential factors (τ_0) of 7.5 × 10–6 (1), 4.4 × 10–6 (5), and 7.4 × 10–7 s (6). These relaxation parameters are in good agreement with other similar NdIII, ErIII, and YbIII field-induced SMM compounds reported in the literature.[16,48,51,52]

Nevertheless, the thermal dependencies of τ for the three compounds at low temperatures deviate from the linearity of the thermal Orbach process. Therefore, these data were fitted by taking into account Raman, direct, and QTM relaxation processes.

The relaxation rate of compound 1 at low temperatures can be simulated by using the expression $\tau^{-1} = CT^n + AT$ with the first term representing the Raman relaxation process and the second the direct relaxation process (Figure 4c). The fitting afforded values of C = 1.03 s–1 K–n, n ≈ 6, and A = 823.60 s–1 K–1. These values are comparable to those found for other NdIII compounds.[53] Although usually n = 9 for Kramers ions, n values between 1 and 6 can be considered acceptable, as a result of the structure of the levels.[51]

For compound 5, the equation $\tau^{-1} = \tau_0^{-1}\exp(-U_{eff}/kBT) + CT^n$, which accounts for Orbach and Raman relaxation processes, reproduces the thermal dependence for the whole temperature range (Figure 4f). The fit leads to values of $\tau_0 = 3.50 \times 10^{-5}$ s, U_{eff} = 2.8 cm–1, and C = 0.82 s–1 K–9 (with parameter n = 9). Nevertheless, because the frequency dependence of the susceptibility appears to be weak, the values extracted from all the fittings of this data should be considered only as a qualitative approach.

In the case of compound 6, the equation $\tau^{-1} = \tau_0^{-1}\exp(-U_{eff}/kBT) + CT^9 + AT$ was used to reproduce the data (Figure 4i). The best-fit values obtained were $\tau_0 = 4.47 \times 10^{-6}$ s, U_{eff} =15.6 cm–1, C = 0.11 s–1 K–9, and A = 16.75 s–1 K–1.

Photoluminescence Studies

The emission properties of complexes 1–6 were studied at room temperature and 77 and 10 K in the solid state. Excitation of the samples at 410 nm induced NIR luminescence of the LnIII ions, assigned to the 4F3/2→4IJ (J = 9/2, 11/2, and 13/2), 4I13/2→4I15/2, and 2F5/2→2F7/2 transitions for NdIII, ErIII, and YbIII, respectively. All the complexes presented residual emission of the ligand in the visible range between 400–500 nm, as depicted in Figure S3 in the Supporting Information.

Ligand-Centered Luminescence

The photophysical properties of complex 3 were investigated in order to study the ligand-centered luminescence, as this complex contains the non-emissive GdIII center. The room-temperature spectrum (Figure 5a) shows a broad emission between 425 and 650 nm with a maximum at 463 nm. The spectrum recorded at 77 K (Figure 5b, red spectrum) presents two bands assigned to the emission from the singlet (455 nm, 21978 cm–1) and triplet (495 nm, 20202 cm–1) excited states.This assignment was confirmed by time-gated measurements (delay of 50 μs) in which only the second emission band was visible (Figure 5b, black spectrum). The low-lying energy of the triplet state prevents the sensitization of TbIII and EuIII, but is compatible with the sensitization of NIR emitters such as NdIII, ErIII, and YbIII.

NdIII-Centered Luminescence

Complex 1 presents the characteristic NdIII emission profile with three main transitions at room temperature (Figure 5c, black line): 4F3/2→4I9/2 at 860 nm, 4F3/2→4I11/2 at 1060 nm, and 4F3/2→4I13/2 at 1310 nm. Cooling down to 77 K (Figure 5c, red line) and 10 K (see Figure S4 in the Supporting Information) strongly increases the resolution of the spectrum. The spectrum at 10 K allowed us to analyze in detail the first transition (4F3/2→4I9/2), and as can be seen in Figure 5d, this emission presents five peaks that correspond to the five expected Stark levels for low-symmetry J = 9/2[54] centered at 876, 888, 896, 903, and 909 nm. This transition gives us information on the crystal-field energy of the neodymium ions in complex 1 and allows us to estimate the energy between the ground and first-excited mJ states of the fundamental 4I9/2 level, about 150 cm–1. The difference between this value and the effective energy barrier value obtained from the Arrhenius fit of the ac data (8.0 cm–1) confirms that relaxation of the magnetization takes place by direct, Raman, and/or QTM processes instead of by a pure Orbach process.[16]

ErIII-Centered Luminescence

Complex 5 presents one main transition that corresponds to the 4I13/2→4I15/2 transition with a maximum at 1537 nm (Figure 5e). Lowering the temperature down to 10 K (see Figure S5 in the Supporting Information) did not increase enough the resolution to allow access to the crystal-field splitting data.

YbIII-Centered Luminescence

Complex 6 presents the characteristic YbIII emission profile, with the main transition 2F5/2→2F7/2 centered at 980 nm (Figure 5f, black spectrum). When lowering the temperature to 77 K (Figure 5f, red line) and even down to 10 K (see Figure S6 in the Supporting Information), the emission band splits into nine bands with maxima (and shoulders) at 980, 1001, 1003, 1007, 1011, 1015, 1017, 1020, 1022, and 1030 nm. This number of contributions is higher than the degeneracy of the 2F7/2 ground state (Kramers' doublets), which has a maximum of four contributions. As the two YbIII ions are crystallographically identical, the additional emission contributions cannot be explained by the presence of two YbIII ions in the complex. The presence of only one phase in the complex was checked by powder XRD (see Figure S7). The presence of additional bands could thus be attributed to additional transitions coming from the second and/or third mJ states of the 2F5/2 multiplet state, by analogy with previous studies by Ouahab et al.[55,56] and Auzey and coworkers,[57] or vibrational contributions. This prevents us from establishing a clear crystal-field energy diagram for this complex.

CONCLUSIONS

Herein we have presented structural, magnetic, and luminescence studies of six new homodinuclear lanthanide compounds based on the use of 9-anthracenecarboxylic acid (9-HAC) and 2,2′-bipyridine (bpy) ligands. We have used a straightforward room-temperature synthetic procedure and have successfully obtained compounds with the formula [Ln2(μ2-9-AC)4(9-AC)2-(bpy)2] [LnIII = Nd (1), Eu (2), Gd (3), Tb (4), Er (5), and Yb (6)] and also the previously published [Dy2(μ2-9-AC)4(9-AC)2(bpy)2] compound.

The NdIII (1), ErIII (5), and YbIII (6) products display the corresponding f–f emission luminescence in the NIR range due to absorption by the ligand followed by energy transfer to the metal.

The fitting of MT versus T to the Heisenberg–Dirac–Van Vleck (HDVV) spin Hamiltonian for the GdIII complex 3 reveals a weak antiferromagnetic interaction between the two LnIII within the dinuclear unit. Additionally, dynamic magnetic measurements revealed field-induced SMM character for compounds 1, 5, and 6, with effective energy barriers of 8.0, 5.6, and 16.4 cm–1, respectively, and pre-exponential factors (τ0) of 7.5 × 10–6 (1), 4.4 × 10–6 (5), and 7.4 × 10–7 s (6).

Thus, compounds 1, 5, and 6 present both field-induced SMM and luminescent properties and can be considered to be multifunctional complexes. A few examples of magnetic and luminescent homometallic dinuclear compounds containing ErIII[58,59] or YbIII[60] ions can be found in the literature but, to the best of our knowledge, compound 1 is the first example of a homodinuclear NdIII complex exhibiting these physical properties.

In the case of compound 1, the higher energy between the first-excited mJ state and the ground mJ state derived from the emission data (ca. 150 cm–1) compared with the effective energy barrier obtained from the Arrhenius fit of the ac magnetic data (8.0 cm–1) confirms that the relaxation of the magnetization does not occur by a pure Orbach process.

EXPERIMENTAL SECTION

Starting Materials: Ln(NO3)3·6H2O salts (Strem Chemicals), 9-anthracenecarboxylic acid (TCI), 2,2′-bipyridine, and pyridine (Aldrich) were used as received without further purification. Physical Measurements Elemental analyses of the compounds were performed at the Serveis Científics i Tecnològics of the Universitat de Barcelona. IR spectra (4000–400 cm–1) were recorded from KBr pellets with a Perkin–Elmer 380-B spectrophotometer. Luminescence spectra were measured by using a Horiba–Jobin–Yvon Fluorolog-3® spectrofluorimeter equipped with a three-slit double-grating excitation and emission monochromator with dispersions of 2.1 nm/mm (1200 grooves/mm). Steady-state luminescence was excited by unpolarized light from a 450 W xenon CW lamp and detected at an angle of 90° for diluted solution measurements and by a red-sensitive Hamamatsu R928 photomultiplier tube for solid-state measurements. Spectra were reference-corrected for both variation of the excitation source light intensity (lamp and grating) and the emission spectral response (detector and grating). NIR spectra were recorded at an angle of 90° by using a liquid-nitrogen-cooled solid indium/gallium/arsenic detector (850–1600 nm). Measurements at 10 K were conducted in a quartz tube by using helium in an Oxford Instrument cryostat (Optistat- CF2).

Magnetic measurements were performed on solid polycrystalline samples in a Quantum Design MPMS-XL SQUID magnetometer at the Magnetic Measurements Unit of the Universitat de Barcelona. Pascal's constants were used to estimate the diamagnetic corrections, which were subtracted from the experimental susceptibilities to give the corrected molar magnetic susceptibilities.

Powder X-ray diffraction data were recorded at the Serveis Científics i Tecnològics of the Universitat de Barcelona with a PANalytical X'Pert PRO MPD θ/θ powder diffractometer of 240 mm radius in a configuration of convergent beam with a focalizing mirror and a transmission geometry with flat samples sandwiched between low absorbing films. Cu-Kα radiation (λ = 1.5418 Å) was used. Work power: 45 kV, 40 mA. Incident beam slits defining a beam height of 0.4 mm. Incident and diffracted beam 0.02 radians. Soller slits PIXcel detector: Active length = 3.347°, 2θ/θ scans from 2 to 70° 2θ with a step size of 0.026° 2θ and a measuring time of 298 s per step.

Syntheses: The dinuclear lanthanide complexes 1–6 were obtained based on the previously proposed synthetic procedure for the [La2(μ2-9-AC)4(9-AC)2(bpy)2] compound.[38] A mixture of 9-anthracenecarboxylic acid (0.05 mmol) and 2,2′-bipyridine (0.05 mmol) in the presence of pyridine (0.05 mL) in methanol (10 mL) was slowly diffused into a test-tube containing a solution of the corresponding Ln(NO3)3·nH2O salt (0.1 mmol) in water (15 mL). Yellow single crystals of the complexes suitable for X-ray analysis appeared after a few days. The previously reported [Dy2(μ2-9-AC)4(9-AC)2(bpy)2] could also be obtained by using this approach.

Data for 1: Selected IR bands (KBr pellet): ν˜ = 1594 (vs), 1517 (s), 1486 (w), 1432 (s), 1387 (s), 1318 (s), 1276 (m), 732 (s) cm–1. C110H70N4Nd2O12 (1928.18): calcd. C 68.52, H 3.66, N 2.91; found C 68.34, H 3.93, N 2.97.

Data for 2: Selected IR bands (KBr pellet): ν˜ = 1600 (vs), 1522 (s), 1488 (w), 1433 (m), 1400 (s), 1321 (s), 1278 (m), 730 (s) cm–1. C110H70Eu2N4O12 (1943.62): calcd. C 67.97, H 3.63, N 2.88; found C 67.96, H 3.69, N 3.06.

Data for 3: Selected IR bands (KBr pellet): ν˜ = 1595 (vs), 1523 (m), 1482 (w), 1433 (m), 1398 (vs), 1317 (s), 1276 (m), 727 (s) cm–1. C110H70Gd2N4O12 (1954.20): calcd. C 67.60, H 3.61, N 2.86; found C 67.26, H 3.39, N 3.02.

Data for 4: Selected IR bands (KBr pellet): ν˜ = 1601 (vs), 1525 (m), 1488 (w), 1434 (m), 1391 (s), 1322 (s), 1279 (m), 730 (s) cm–1. C110H70N4O12Tb2 (1957.56): calcd. C 67.49, H 3.60, N 2.86; found C 67.38, H 3.62, N 2.97.

Data for 5: Selected IR bands (KBr pellet): ν˜ = 1604 (vs), 1530 (m), 1487 (w), 1436 (m), 1388 (m), 1321 (s), 1277 (w), 731 (s) cm–1. C110H70Er2N4O12 (1974.22): calcd. C 66.92, H 3.57, N 2.84; found C 66.41, H 3.96, N 2.85.

Data for 6: Selected IR bands (KBr pellet): ν˜ = 1610 (vs), 1532 (m), 1488 (w), 1452 (m), 1387 (m), 1322 (s), 1277 (w), 731 (s) cm–1. C110H70N4O12Yb2 (1985.78): calcd. C 66.53, H 3.55, N 2.82; found C 66.58, H 3.47, N 2.81.

X-ray Crystallography

Crystals of 1–6 were mounted in air on a D8VENTURE (Bruker) diffractometer equipped with a CMOS detector. The crystallographic data and details of the intensity data collection and structural refinements are presented in Table 1. All the structures were refined by the least-squares method. Intensities were collected by using multilayer monochromated Mo-Kα radiation. Lorentz polarization and absorption corrections were made for all samples. The structures were solved by direct methods using the SHELXS-97 computer program[61] and refined by full-matrix least-squares methods using the SHELXL-2014 computer program.[62] The non-hydrogen atoms were located in successive difference Fourier syntheses and refined with anisotropic thermal parameters on F2. For hydrogen atoms, isotropic temperature factors have been assigned as 1.2 or 1.5 times the respective parent.

CCDC 1590414 (for 1), 1590415 (for 2), 1590449 (for 3), 1590451 (for 4), 1590450 (for 5), and 1590452 (for 6) contain the supplementary crystallographic data for this paper. These data can be obtained free of charge from The Cambridge Crystallographic Data Centre.

ACKNOWLEDGEMENTS

R. V., B. C., M. S. E. F., and S. S. acknowledge the financial support from the Spanish government (Grant CTQ2015-63614-P). S. S. acknowledges the financial support from the "Obra Social de la Fundació Bancària La Caixa" and "La Fundació Universitaria Agustí Pedro i Pons". O. M. and S. S. acknowledge the ANR (French National Research Agency) for financial support (granted collaborative project ANR-15-CE29-0019).

REFERENCES

[1] X. F. Tan, J. Zhou, H. H. Zou, L. Fu, Q. Tang, Inorg. Chem. 2017, 56, 10361–10369.

[2] H.-Y. Shen, W.-M. Wang, H.-L. Gao, J.-Z. Cui, RSC Adv. 2016, 6, 34165–34174.

[3] S. G. Reis, M. Briganti, S. Soriano, G. P. Guedes, S. Calancea, C. Tiseanu, M. A. Novak, M. A. Del Águila-Sánchez, F. Totti, F. Lopez-Ortiz, M. Andruh, M. G. F. Vaz, Inorg. Chem. 2016, 55, 11676–11684.

[4] J. D. Rinehart, J. R. Long, Chem. Sci. 2011, 2, 2078.

[5] R. A. Layfield, M. Murugesu (Eds.), Lanthanides and Actinides in Molecular Magnetism, Wiley-VCH, Weinheim, 2015.

[6] D. Aguilà, L. A. Barrios, V. Velasco, O. Roubeau, A. Repollés, P. J. Alonso, J. Sesé, S. J. Teat, F. Luis, G. Aromí, J. Am. Chem. Soc. 2014, 136, 14215–14222.

[7] M. Affronte, J. Mater. Chem. 2009, 19, 1731–1737.

[8] L. Bogani, W. Wernsdorfer, Nat. Mater. 2008, 7, 179–186.

[9] L. Sorace, C. Benelli, D. Gatteschi, Chem. Soc. Rev. 2011, 40, 3092.

[10] D. A. Atwood (Ed.), The Rare Earth Elements: Fundamentals and Applications, John Wiley & Sons Ltd., Chichester, 2005.

[11] J. Tang, P. Zhang, Lanthanide Single Molecule Magnets, Springer, Berlin Heidelberg, 2015.

[12] F. S. Guo, B. M. Day, Y. C. Chen, M. L. Tong, A. Mansikkamäki, R. A. Layfield, Angew. Chem. Int. Ed. 2017, 56, 11445–11449; Angew. Chem. 2017, 129, 11603.

[13] C. A. P. Goodwin, F. Ortu, D. Reta, N. F. Chilton, D. P. Mills, Nature 2017, 548, 439–442.

[14] S. Da Jiang, B. W. Wang, H. L. Sun, Z. M. Wang, S. Gao, J. Am. Chem. Soc. 2011, 133, 4730–4733.

[15] J. Y. Ge, L. Cui, J. Li, F. Yu, Y. Song, Y. Q. Zhang, J. L. Zuo, M. Kurmoo, Inorg. Chem. 2017, 56, 336–343.

[16] F. Pointillart, O. Cador, B. Le Guennic, L. Ouahab, Coord. Chem. Rev. 2017, 346, 150–175.

[17] A. K. Jassal, B. S. Sran, Y. Suffren, K. Bernot, F. Pointillart, O. Cador, G. Hundal, Dalton Trans. 2018, 47, 4722–4732.

[18] A. K. Jassal, N. Aliaga-Alcalde, M. Corbella, D. Aravena, E. Ruiz, G. Hundal, Dalton Trans. 2015, 44, 15774–15778 .

[19] J. D. Rinehart, M. Fang, W. J. Evans, J. R. Long, J. Am. Chem. Soc. 2011, 133, 14236–14239.

[20] T. Morita, M. Damjanović, K. Katoh, Y. Kitagawa, N. Yasuda, Y. Lan, W. Wernsdorfer, B. K. Breedlove, M. Enders, M. Yamashita, J. Am. Chem. Soc. 2018, 140, 2995–3007.

[21] F. Habib, M. Murugesu, Chem. Soc. Rev. 2013, 42, 3278–3288.

[22] S. V. Eliseeva, J.-C. G. Bünzli, Chem. Soc. Rev. 2010, 39, 189–227.

[23] A. D'Aléo, F. Pointillart, L. Ouahab, C. Andraud, O. Maury, Coord. Chem. Rev. 2012, 256, 1604–1620.

[24] W. Xu, T. K. Lee, B.-S. Moon, D. Zhou, H. Song, Y.-J. Kim, S. K. Kwak, P. Chen, D.-H. Kim, V. Y. Panchenko, Nanoscale 2017, 9, 9238–9245.

[25] C.-H. Huang, Rare Earth Coordination Chemistry: Fundamentals and Applications, Wiley, Singapore, 2010.

[26] A. Ouchi, Y. Suzuki, Y. Ohki, Y. Koizumi, Coord. Chem. Rev. 1988, 92, 29–43.

[27] N. C. Anastasiadis, D. A. Kalofolias, A. Philippidis, S. Tzani, C. Raptopoulou, V. Psycharis, C. J. Milios, A. Escuer, S. P. Perlepes, Dalton Trans. 2015, 44, 10200–10209.

[28] Z. Chen, M. Fang, X. Kang, Y. Hou, B. Zhao, Dalton Trans. 2016, 45, 85–88.

[29] Y. L. Wang, C. B. Han, Y. Q. Zhang, Q. Y. Liu, C. M. Liu, S. G. Yin, Inorg. Chem. 2016, 55, 5578–5584.

[30] L. Song, J. Gao, J. Mol. Struct. 2013, 1032, 207–211.

[31] B. Casanovas, F. Zinna, L. Di Bari, M. S. El Fallah, M. Font-Bardía, R. Vicente, Dalton Trans. 2017, 46, 6349–6357.

[32] K. P. Carter, K. E. Thomas, S. J. A. Pope, R. J. Holmberg, R. J. Butcher, M. Murugesu, C. L. Cahill, Inorg. Chem. 2016, 55, 6902–6915.

[33] B. Branchi, P. Ceroni, V. Balzani, F. G. Klärner, F. Vögtle, Chem. Eur. J. 2010, 16, 6048–6055.

[34] M. A. Palacios, S. Titos-Padilla, J. Ruiz, J. M. Herrera, S. J. A. Pope, E. K. Brechin, E. Colacio, Inorg. Chem. 2014, 53, 1465–1474.

[35] A. J. Calahorro, I. Oyarzabal, B. Fernández, J. M. Seco, T. Tian, D. Fairen- Jimenez, E. Colacio, A. Rodríguez-Diéguez, Dalton Trans. 2016, 45, 591–598.

[36] J. Long, Y. Guari, R. A. S. Ferreira, L. D. Carlos, J. Larionova, Coord. Chem. Rev. 2018, 363, 57–70.

[37] X. Yi, K. Bernot, F. Pointillart, G. Poneti, G. Calvez, C. Daiguebonne, O. Guillou, R. Sessoli, Chem. Eur. J. 2012, 18, 11379–11387.

[38] C.-S. Liu, L.-F. Yan, Z. Chang, J.-J. Wang, Acta Crystallogr., Sect. E: Struct. Rep. Online 2008, 64, m15–m16.

[39] S. Alvarez, P. Alemany, D. Casanova, J. Cirera, M. Llunell, D. Avnir, Coord. Chem. Rev. 2005, 249, 1693–1708.

[40] J. Cirera, E. Ruiz, S. Alvarez, Inorg. Chem. 2008, 47, 2871–2889. [41] L. E. Ballentine, D. Griffiths, Am. J. Phys. 1991, 59, 1153–1154.

[42] T. Q. Liu, P. F. Yan, F. Luan, Y. X. Li, J. W. Sun, C. Chen, F. Yang, H. Chen, X. Y. Zou, G. M. Li, Inorg. Chem. 2015, 54, 221–228.

[43] Y.-L. Li, Q.-Y. Liu, C.-M. Liu, Y.-L. Wang, L. Chen, Aust. J. Chem. 2015, 68, 488.

[44] N. F. Chilton, R. P. Anderson, L. D. Turner, A. Soncini, K. S. Murray, J. Comput. Chem. 2013, 34, 1164–1175.

[45] F. Cimpoesu, F. Dahan, S. Ladeira, M. Ferbinteanu, J. P. Costes, Inorg. Chem. 2012, 51, 11279–11293.

[46] A. Rohde, W. Urland, Inorg. Chim. Acta 2006, 359, 2448–2454.

[47] W.-H. Zhu, X. Xiong, C. Gao, S. Li, Y. Zhang, J. Wang, C. Zhang, A. K. Powell, S. Gao, Dalton Trans. 2017, 46, 14114–14121.

[48] See ref.[42]

[49] S. M. J. Aubin, Z. Sun, L. Pardi, J. Krzystek, K. Folting, L.-C. Brunel, A. L. Rheingold, G. Christou, D. N. Hendrickson, Inorg. Chem. 1999, 38, 5329–5340.

[50] Y.-N. Guo, G.-F. Xu, Y. Guo, J. Tang, Dalton Trans. 2011, 40, 9953.

[51] A. J. Calahorro, I. Oyarzabal, B. Fernández, J. M. Seco, T. Tian, D. Fairen-Jimenez, E. Colacio, A. Rodríguez-Diéguez, Dalton Trans. 2016, 45, 591–598.

[52] J. J. Le Roy, S. I. Gorelsky, I. Korobkov, M. Murugesu, Organometallics 2015, 34, 1415–1418.

[53] M. V. Marinho, D. O. Reis, W. X. C. Oliveira, L. F. Marques, H. O. Stumpf, M. Déniz, J. Pasán, C. Ruiz-Pérez, J. Cano, F. Lloret, M. Julve, Inorg. Chem. 2017, 56, 2108–2123.

[54] J.-C. G. Bünzli, S. V. Eliseeva in Lanthan. Lumin. Photophysical, Anal. Biol. Asp. (Eds.: P. Hänninen, H. Härmä), Springer Series on Fluorescence, 2010, pp. 1–45.

[55] G. Cosquer, F. Pointillart, B. Le Guennic, Y. Le Gal, S. Golhen, O. Cador, L. Ouahab, Inorg. Chem. 2012, 51, 8488–8501.

[56] S. Speed, M. Feng, G. Fernandez Garcia, F. Pointillart, B. Lefeuvre, F. Riobé, S. Golhen, B. Le Guennic, F. Totti, Y. Guyot, O. Cador, O. Maury, L. Ouahab, Inorg. Chem. Front. 2017, 4, 604–617.

[57] P. Goldner, F. Pell, D. Meicheninb, F. Auzey, J. Lumin. 1997, 71, 137–150.

[58] J.-H. Jia, Q.-W. Li, Y.-C. Chen, J.-L. Liu, M.-L. Tong, Coord. Chem. Rev. 2017, https://doi.org/10.1016/j.ccr.2017.11.012.

[59] P. Martín-Ramos, L. C. J. Pereira, J. T. Coutinho, F. Koprowiak, H. Bolvin, V. Lavín, I. R. Martín, J. Martín-Gil, M. R. Silva, New J. Chem. 2016, 40, 8251–8261.

[60] F. Pointillart, B. Le Guennic, S. Golhen, O. Cador, O. Maury, L. Ouahab, Chem. Commun. 2013, 49, 615–617.

[61] G. M. Sheldrick, Acta Crystallogr., Sect. A 2008, 64, 112–122.

[62] G. M. Sheldrick, Acta Crystallogr., Sect. C: Struct. Chem. 2015, 71, 3–8.

Legends to figures

Figure. 1 a) Partially labeled plot of compound 1. Hydrogen atoms have been omitted for clarity. (b) Coordination polyhedron of the NdIII ions in compound 1.

Scheme 1 Representation of the different coordination modes of the 9-AC ligand.

Figure.2 Representation of the supramolecular arrangement of compound 1 in the (111) plane. π-stacking interactions are represented in blue.

Figure.3. a) MT vs. T plots for compounds 1–6. The blue solid line represents the best fit for complex 3 (see text). (b) Plots of the field dependence of the magnetization for compounds 1 and 3–6.

Figure.4 Frequency dependence of M″ for 1 (a), 5 (d), and =6 (g). Cole–Cole plots for 1 (b), 5 (e), and 6 (h). Solid lines represent the fitting using generalized Debye models. Magnetization relaxation time [ln (τ)] vs. T–1 for 1 (c), 5 (f), and 6 (i). Solid lines represent the theoretical fittings (see text).

Figure.5 (a) Emission spectrum of complex 3 at λex = 360 nm at room temperature in the solid state. (b) Steady-state (in red) and time-gated (in black, baseline-corrected, delay = 50 μs) emission spectra of complex 3 at λex = 360 nm at 77 K in the solid state. (c) Emission spectra of complex 1 at λex = 410 nm at room temperature (black) and 77 K (red) in the solid state. (d) Experimental spectrum () and deconvolution into five Gaussian contibutions of the 4F3/2→4I9/2 band in compound 1 at 10 K. (e) Emission spectra of complex 5 at λex = 410 nm at room temperature (black) and 77 K (red) in the solid state. (f) Emission spectra of complex 6 at λex = 410 nm at room temperature (black) and 77 K (red) in the solid state.

FIGURE 1

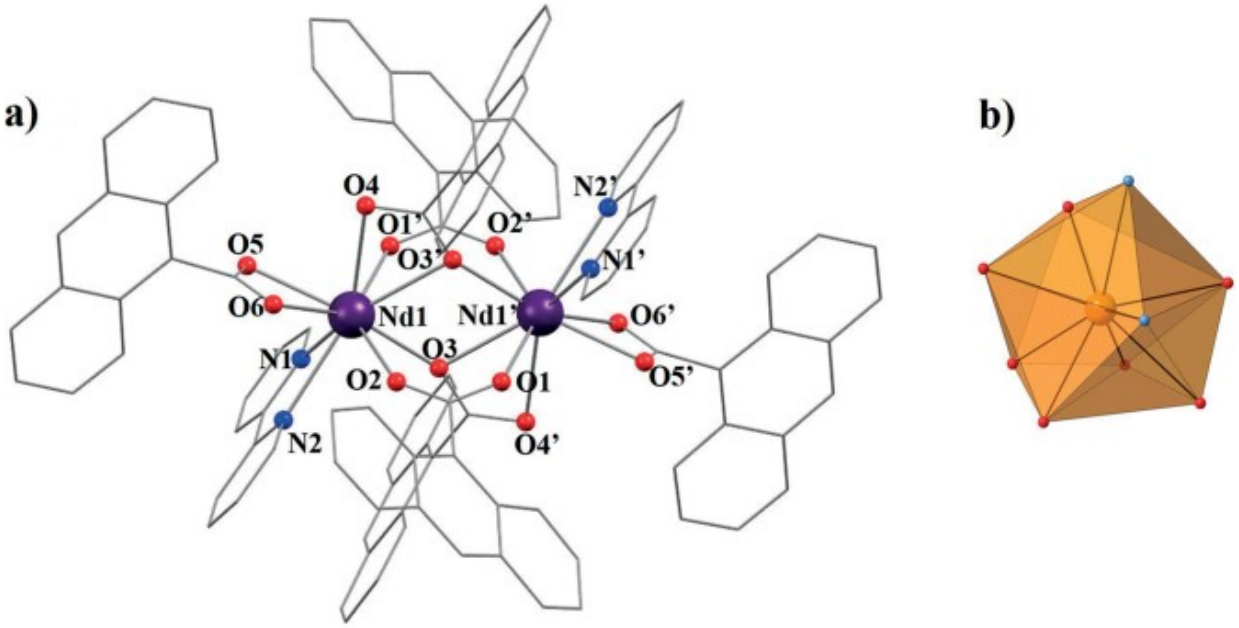

SCHEME 1

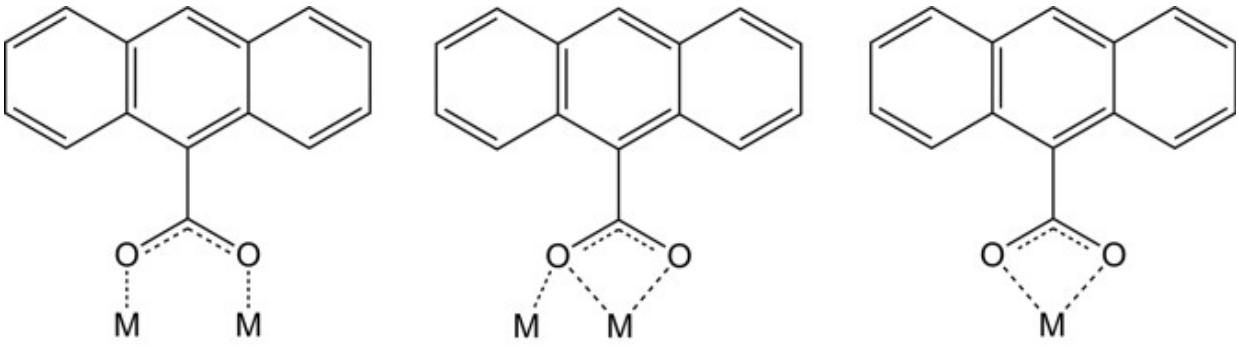

a) *syn, syn* bridge b) chelating-bridging c) chelating

FIGURE 2

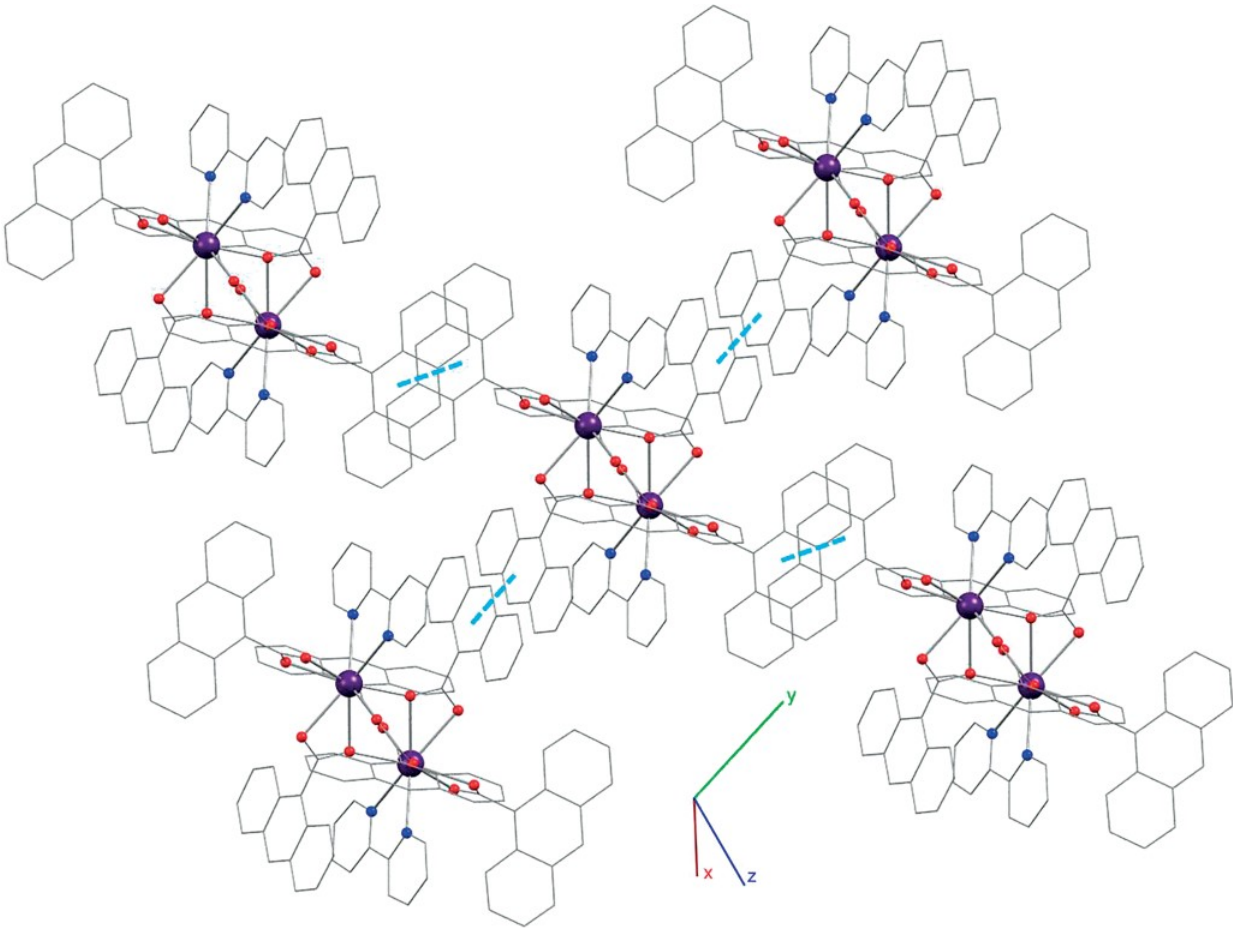

560 **FIGURE 3**

561

562

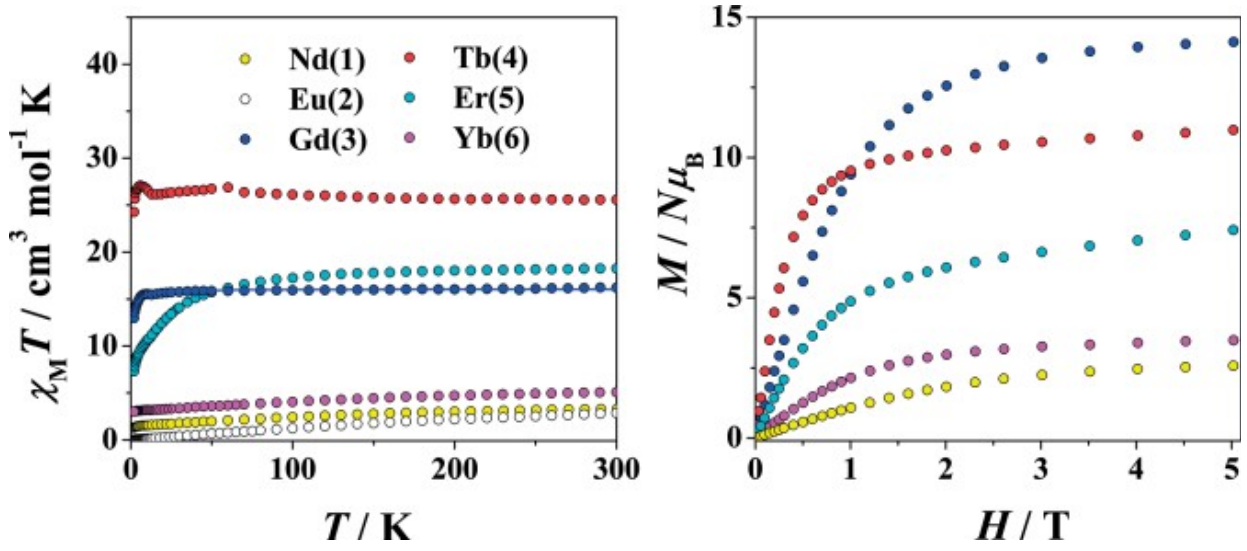

563

564

FIGURE 4

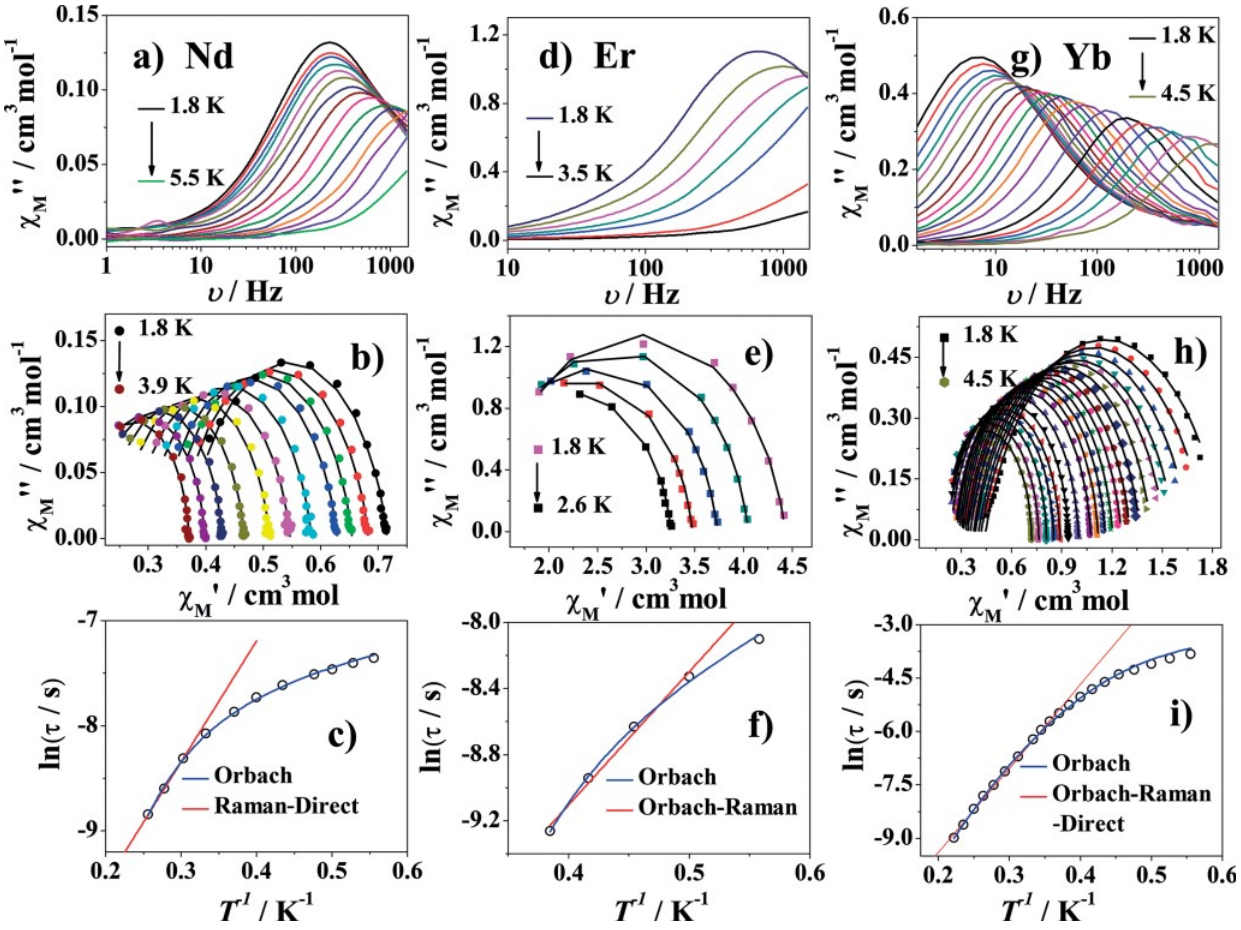
a) Nd
1.8 K
5.5 K
d) Er
1.8 K
3.5 K
g) Yb
1.8 K
4.5 K
b)
1.8 K
3.9 K
e)
1.8 K
2.6 K
h)
1.8 K
4.5 K
c)
Orbach
Raman-Direct
f)
Orbach
Orbach-Raman
i)
Orbach
Orbach-Raman
-Direct
χM'' / cm3mol-1
χM' / cm3mol
υ / Hz
ln(τ / s)
T-1 / K-1

570 **FIGURE 5**

571

572

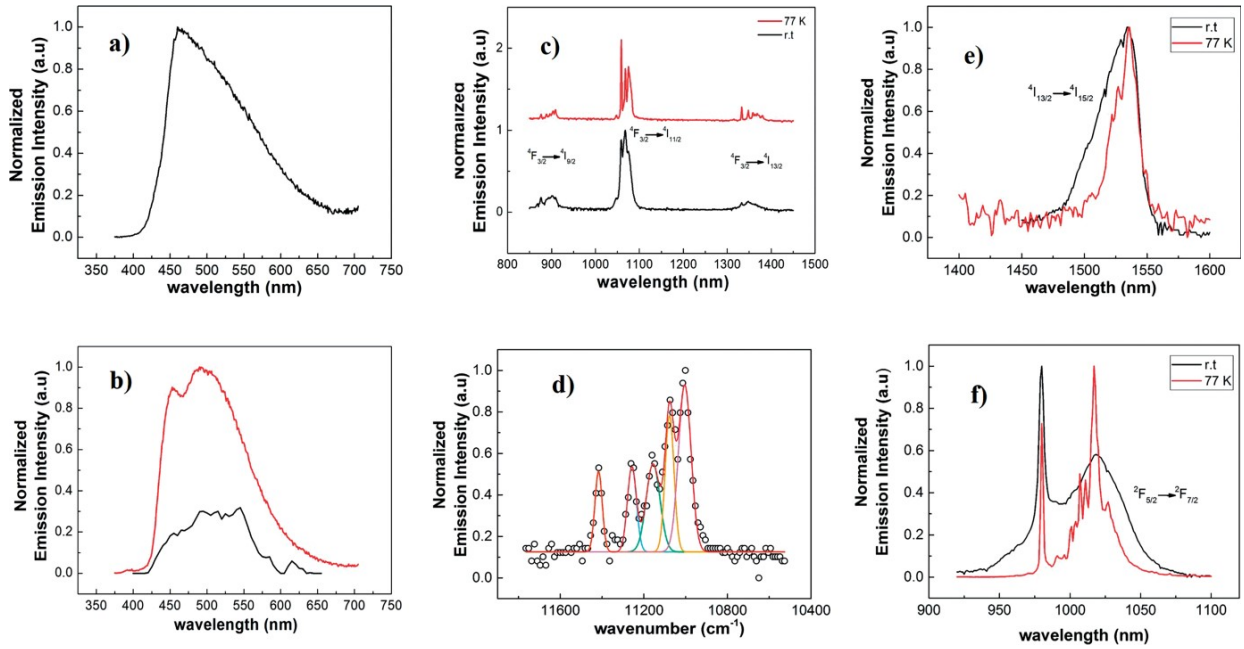

573

574

575 **Table 1.** Crystal data and data collection details for the X-ray structures of complexes 1–6.

576

Table 1. Crystal data and data collection details for the X-ray structures of complexes **1–6**.

	1	**2**	**3**	**4**	**5**	**6**
Formula	$C_{110}H_{70}Nd_2N_4O_{12}$	$C_{110}H_{70}Eu_2N_4O_{12}$	$C_{110}H_{70}Gd_2N_4O_{12}$	$C_{110}H_{70}Tb_2N_4O_{12}$	$C_{110}H_{70}Er_2N_4O_{12}$	$C_{110}H_{70}Yb_2N_4O_{12}$
M_r	1928.18	1943.62	1954.20	1957.56	1974.22	1985.78
System	triclinic	triclinic	triclinic	triclinic	triclinic	triclinic
Space group	*F*(000)	*F*(000)	*F*(000)	*F*(000)	*F*(000)	*F*(000)
a [Å]	11.9069(4)	11.8747(6)	12.2974(9)	11.8596(2)	11.7813(4)	11.7650(6)
b [Å]	13.3817(5)	13.4607(7)	13.8404(11)	13.5247(2)	13.5709(6)	13.6275(7)
c [Å]	15.3555(6)	15.3005(6)	14.5621(11)	15.1751(3)	15.1192(6)	15.0737(7)
α [°]	113.130(2)	108.514(3)	66.483(3)	108.626(1)	109.426(2)	109.790(2)
β [°]	103.680(2)	110.459(3)	69.688(4)	110.888(1)	110.382(1)	110.311(2)
γ [°]	102.614(2)	101.567(3)	69.254(3)	100.768(1)	100.427(2)	100.270(2)
V [Å^3]	2049.21(14)	2034.87(19)	2063.3(3)	2026.86(7)	1974.22	2009.21(18)
Z	1	1	1	1	1	1
T [K]	100(2)	100(2)	100(2)	100(2)	100(2)	100(2)
λ(Mo-K_α) [Å]	0.71073	0.71073	0.71073	0.71073	0.71073	0.71073
$D_{calcd.}$ [g cm^{-3}]	1.563	1.586	1.573	1.604	1.629	1.641
μ(Mo-K_α) [mm^{-1}]	1.326	1.601	1.666	1.805	2.145	2.388
R	0.0210	0.0278	0.0393	0.0253	0.0156	0.0142
wR_2	0.0466	0.0594	0.0965	0.0551	0.0367	0.0364

577

578

579 **Table 2** Selected bond lengths [Å] for compounds 1–6.

580

	1	2	3	4	5	6
Ln1–O2	2.4388(15)	2.3396(14)	2.354(3)	2.3076(11)	2.2734(10)	2.2513(10)
Ln1–O3	2.6074(15)	2.6064(17)	2.579(4)	2.6089(14)	2.6562(11)	2.7473(11)
Ln1–O4	2.6426(16)	2.585(2)	2.597(3)	2.5544(15)	2.4838(13)	2.4508(13)
Ln1–O5	2.4544(16)	2.4493(14)	2.395(3)	2.4141(12)	2.3952(10)	2.3647(10)
Ln1–O6	2.4897(14)	2.4166(18)	2.455(3)	2.3988(15)	2.3616(12)	2.3448(12)
Ln1–N1	2.6744(18)	2.622(2)	2.619(4)	2.5925(17)	2.5522(13)	2.5339(13)
Ln1–N2	2.6580(18)	2.648(2)	2.612(4)	2.6182(16)	2.5876(13)	2.5733(13)
Ln1–O1′	2.3856(14)	2.3909(16)	2.363(3)	2.3690(13)	2.3269(11)	2.3021(10)
Ln1–O3′	2.3910(15)	2.3429(16)	2.349(3)	2.3086(13)	2.2610(11)	2.2192(10)
Ln1–Ln1′	3.9960(4)	3.9553(4)	3.9215(5)	3.9338(4)	3.9278(4)	3.9584(4)
Symmetry	2 − *x*, 1 − *y*, 1 − *z*	1 − *x*, 1 − *y*, 1 − *z*	1 − *x*, −*y*, 2 − *z*	−*x*, −*y*, −*z*	1 − *x*, 1 − *y*, 1 − *z*	1 − *x*, 1 − *y*, 1 − *z*

581